



Iranian Research Organization
for Science and Technology
(IROST)

Advances
Environmental
Technology



Journal home page: <https://aet.irost.ir/>

Response surface methodology analysis of the photodegradation of methyl orange dye using synthesized TiO₂/Bentonite/ZnO composites

Aazam Dinari, Jafar Mahmoudi*

School of Chemistry, Damghan University, Damghan, Iran

ARTICLE INFO

Document Type:
Research Paper

Article history:
Received 14 September 2021
Received in revised form
21 February 2022
Accepted 21 February 2022

Keywords:

TiO₂
Bentonite
Zinc oxide
Methyl orange
Response surface
methodology

ABSTRACT

In this research, a modified TiO₂/Bentonite (Be) composite with various values of zinc oxide was used as a photocatalyst in the degradation of methyl orange as a dye pollutant. The synthesized composites were characterized by X-ray diffraction (XRD), Field emission scanning electron microscopy (FESEM), Fourier transform infrared spectroscopy (FTIR), X-ray fluorescence (XRF), and Thermal gravimetric analysis (TGA). The results showed that the composite synthesized by 6.5% zinc oxide had the highest anatase phase and appropriate thermal stability. Moreover, the simultaneous effect of different parameters was investigated using the central composite (CC) design defined under response surface methodology (RSM). The results showed that the polynomial model obtained from the analysis of variance (ANOVA) correctly predicted the experimental data. The optimal conditions of dye degradation for the synthesized composite with 6.5% zinc oxide using 4 g/L of photocatalyst for 30 minutes at a pH=5 and a dye concentration of 20 ppm had the highest degradation percentage equal to 95% with a high desirability of 0.981. Also, the photocatalytic activity of TiO₂/Be/ZnO (6.5%) in certain conditions for reuse in five consecutive steps showed a slight decrease in the degradation of methyl orange.

1. Introduction

The global demand for wholesome water along with an increase in the concentration of non-biodegradable pollutants necessitates the improvement of industrial wastewater treatment methods. Industries such as textile, pharmacy, and leather manufacturing have a large amount of dye materials and produce dye pollutants that enter into the environment; among the aforementioned

cases, the textile industry is the largest manufacturer of dye pollutant [1-4]. The disadvantages of the presence of dyes in water resources include reduced light penetration, allergies, genetic mutations, low biological degradation, and production of amine groups in anaerobic degradation (carcinogenicity). According to reports [5-6], there are thousands of types of commercial dyes found in the world, a part of which enters industrial wastewater due to the

*Corresponding author: +98 233 522 0095

E-mail: mahmoudi@du.ac.ir

DOI: 10.22104/AET.2022.5204.1409

lack of stabilization of dye molecules on fibers and inefficiency of dyeing units. An example is azo dyes, a large class of synthetic organic dyes that contain nitrogen as the azo group $-N=N-$ as part of their molecular structures, and they are not easily degraded in wastewater. According to environmental standards, the dye wastewater should be optimally purified before discharging it into the environment. There are various methods for decolorization of textile industry waste, including coagulation, chemical oxidation, biological purification, ion exchange, adsorption, and combined processes such as ozonation and coagulation, or ion exchange [7-8]. Extensive research has been carried out recently on removing of such pollutants using photocatalyst materials. Photocatalytic degradation is an effective, beneficial, and cost-effective method with the least pollution. Titanium dioxide is one of the materials that has been widely used as a photocatalyst semiconductor material. One of the advantages of this semiconductor is its physical and chemical stability and relatively inexpensive price. Titanium dioxide is a white, non-toxic, and environmentally friendly material that facilitates the production of hydroxyl radicals with the adsorption of photons with a certain wavelength and electron-hole production [9]. Problems such as the separation of nanoparticles and low-efficiency value in photocatalytic reactions, due to the electron-hole recombination, limits the beneficial use of titanium dioxide. In fact, a large number of electron-hole pairs are recombined, and a small number migrate to the photocatalyst surface and participate in the oxidation-reduction processes [10]. To overcome such problems, the stabilization of titanium dioxide on the proper base and doping with other semiconductors is suggested. One of the semiconductors that can increase the photocatalytic activity of titanium dioxide is zinc oxide. Moreover, mineral compounds such as different types of clay are appropriate for connecting to titanium dioxide due to their unique structure, pores, uniform channels, and very good absorption ability [11-12]. Bentonite is mainly composed of montmorillonite. This type of clay has a greasy and soap-like surface. In the chemical structure of montmorillonite, the replacement of Al^{3+} for Si^{4+} in the tetrahedral layers and the

replacement of Mg^{2+} and Zn^{2+} in the octagonal layers causes a net negative charge on the soil surface. The imbalance of electrical charge is neutralized and compensated by internal cations (mainly Na^+ and Ca^{2+}); as a result, montmorillonite finds physical-chemical properties such as high contact surfaces, excellent absorption power, high structural stability, and strong capacity to cause suspensions at low concentrations [13]. On the other hand, the coupling of two semiconductors (titanium dioxide, zinc oxide) with different a capacity band and energy levels leads to the separation of an effective charge. If one of the semiconductors is exposed to radiation, after formation of the electron and hole, the electron generated in the active semiconductor is transferred to the conductive band of the other semiconductor. Hence, the amount of electron-hole recombination is reduced, and as a result, the amount of pollutant degradation, in this case, will be increased [14]. Based on our findings, the application of TiO_2 modified with bentonite and ZnO for methyl orange dye degradation has yet to be studied. The aim of the present work is to synthesize and characterize $TiO_2/Be/ZnO$ and study their use in the photolytic degradation of methyl orange dye using RSM. The prepared photocatalysts were characterized using XRD, XRF, FESM, TGA and FT-IR techniques. The impact of effective parameters such as time of degradation reaction, amount of photocatalyst, pollutant concentration, and pH of solution were investigated for the degradation of methyl orange dye via design of experiment using the central composite design defined under response surface methodology (RSM). The photocatalytic degradation of methyl orange dye was measured using an absorption spectrophotometer UV-Vis.

2. Materials and methods

2.1. Materials

Titanium isopropoxide (97%, Aldrich), ethanol (99%, Merck), acetic acid (99.5%, Merck), zinc nitrate (98%, Merck), sodium hydroxide (98%, Merck), distilled water, and bentonite from the Shiraz region were used for preparing the composites. Methyl orange (99%, Merck) was used to investigate photocatalytic activity.

2.2. Preparing TiO₂/Be/ZnO composites

For preparing TiO₂/Be/ZnO, the titanium dioxide solution was prepared by mixing 5 mL of titanium isopropoxide and 20 mL of ethanol via the sol-gel method at room temperature. After constant stirring for half an hour, a mixture containing acetic acid, water, and ethanol was added to the initial solution. The resulting solution was subjected to magnetic stirring for 60 min, and a clear yellow solution was obtained [15]. For the synthesis of the TiO₂/Be composite, a certain amount of bentonite was added to the TiO₂ solution and stirred for six hours on a magnetic stirrer. According to the results of our primary experiments, the optimum bentonite content obtained was equal to 4 wt% in the TiO₂/Be composite. For synthesis of the TiO₂/Be/ZnO composite, 4 wt% bentonite was added to the TiO₂ solution. After three hours of constant stirring, different amounts of zinc nitrate were added to the above solution to obtain the optimum amount of zinc oxide and stirred for 6 hours on a magnetic stirrer. Afterwards, a solution of water and ethanol was separately added to the above solution drop by drop in equal proportions using a burette until the gel was formed. The resulting gel was left at room temperature for 24 hours and then dried in an oven at 120°C for 4 hours. For the formation of crystalline particles, the resulting powder was calcined in the furnace at a temperature of 300°C for four hours [16-17].

2.3. Characterization of prepared composites

XRD, D8-Advance Bruker Cu K α (λ = 0.15406 nm), was used to determine the structure of the prepared samples in the angle range of 10-80 degrees. X-ray fluorescence (XRF), S4 Explorer Bruker, was used to identify the elements in the prepared samples. The chemical properties and surface functional groups of the prepared composites were evaluated using the Perkin Elmer spectrum RXI FT-IR system. The morphology of the particle surface was examined using FE-SEM, HTACHI S-4160, with a magnification of 20-30000 and maximum voltage of 30KV. In order to examine the thermal stability of the particles, a thermogravimetric analysis (TGA) device, namely the Bahr thermo Analyse STA 503, was used at a temperature range of 25-800°C, 10°C per minute.

2.4. Photocatalytic experiments

Methyl orange dye was selected as a pollutant to evaluate the photocatalytic activity of different composites. To this end, 0.1g of the composite was added to 25 mL of dye solution at a specific concentration. To investigate the photocatalytic activity, a reactor equipped with a mercury vapor lamp of 250 W and a magnetic stirrer was used to ensure complete mixing of the dye material and composites. The pH of the solution was adjusted by sodium hydroxide and hydrochloric acid. After the reaction, for the removal of catalytic turbidity, the samples were first passed through the filter; then, they were centrifuged for 60 minutes. In the end, the samples were prepared to measure the changes in dye intensity. The UV-Vis spectrophotometer, Lambda-25 manufactured by Perkin Elmer, was used to evaluate the absorption spectrum of samples. A spectrum of a solution of methyl orange showed a maximum absorbance in the visible region at 464 nm. This wavelength was used to construct a calibration curve of absorbance vs. concentration of methyl orange to find the linear range of methyl orange absorbance. For the quantitative evaluation of the performance of photocatalysts, the pollutant removal percentage parameter is used, which is defined as:

$$D \% = \frac{A_0 - A_t}{A_0} \times 100 \quad (1)$$

where A_0 means the absorbency of the original solution and A_t means the absorbency of the methyl orange solution after treating for t hours.

2.5. Design of experiment using response surface methodology

In order to investigate the simultaneous effect of catalyst concentration, dye concentration, contact time, and pH, 30 experiments were designed based on the Central Composite Design (CCD) of the RSM method using Design Expert v.10. In the response surface method, using a set of useful statistical and mathematical techniques, the problems in which one or more dependent variables are affected by several independent variables are analyzed. The purpose of this method is to save time and materials, as well as solution optimization. In the experiments designed for photocatalytic degradation of methyl orange, 2-4

g/L of catalyst, the dye concentration range of 10-20 ppm, light exposure of the solution for 30-60 min, and the pH range of 4-9 were considered.

Table 1 shows the design of the experiment carried out by the RSM method and the experimental and predicted results.

Table 1. Experimental conditions and results of RSM for degradation of methyl orange using TiO₂/Be/ZnO composite as photocatalyst.

Run	Photocatalytic operating parameters				Response
	Photocatalyst dosage (g/L)	Time (min)	Dye concentration (ppm)	pH	Degradation percentage (%)
1	2	30	10	5	42.09
2	4	30	10	5	64.1
3	2	60	10	5	31.16
4	4	60	10	5	42.2
5	2	30	20	5	75.1
6	4	30	20	5	92.67
7	2	60	20	5	46.22
8	4	60	20	5	59.93
9	2	30	10	9	40.43
10	4	30	10	9	58.98
11	2	60	10	9	24.72
12	4	60	10	9	35.75
13	2	30	20	9	63.54
14	4	30	20	9	79.29
15	2	60	20	9	35.98
16	4	60	20	9	52.65
17	1	45	15	7	28.4
18	5	45	15	7	62.43
19	3	15	15	7	98.66
20	3	75	15	7	5.65
21	3	45	5	7	25.65
22	3	45	25	7	64.18
23	3	45	15	3	66.39
24	3	45	15	11	33.87
25	3	45	15	7	53.61
26	3	45	15	7	53.61
27	3	45	15	7	53.61
28	3	45	15	7	53.61
29	3	45	15	7	53.61
30	3	45	15	7	53.61

3. Results and discussion

3.1. Characterization of synthesized photocatalysts

3.1.1. X-Ray diffraction

Figure 1 shows the X-ray diffraction spectrum of titanium dioxide (TiO₂), bentonite, and various synthesized samples of TiO₂/Be/ZnO composites. The structural analysis of titanium dioxide particles shows that the spectrum of these particles has certain peaks. The peaks observed at 2θ of 25.52° (101), 38.6° (112), and 48° (200) are related to the

anatase phase [19-18]. The peaks observed at 55° are related to the rutile phase. Given the intensity of the XRD peaks related to titanium dioxide, the anatase phase is the dominant phase. According to other researchers' reports, the rutile phase is always the most stable, but in the case of particles with a diameter less than 14 nm, the anatase phase is more thermodynamically stable. Moreover, from among the crystalline structures of titanium dioxide, the anatase phase is known as the most active phase in terms of photocatalytic activity [20]. In the Bentonite spectrum, the peaks related

to the calcite emerge at 61°, which confirms the calcium content of bentonite. The peaks emerging at 21°, 36°, and 54° are related to montmorillonite. The peak appearing at 27° is attributed to quartz [21].

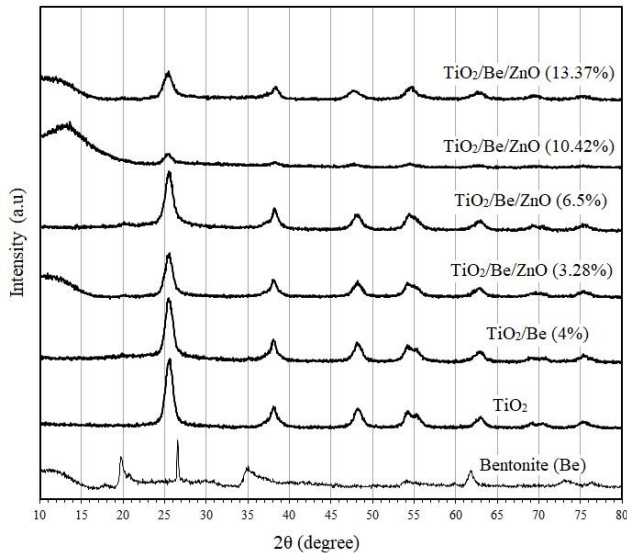


Fig. 1. The X-ray diffraction patterns for the synthesized samples.

In Figure 1, the XRD spectrum of TiO₂/Be (4%) composite is also shown. The resulting spectrum is fully similar to the titanium dioxide spectrum, and almost no side-product that can be attributed to bentonite is seen. In these spectra, the anatase phase is known as the dominant phase. In the TiO₂/Be (4%) sample, the titanium dioxide peaks have small displacements, and the shift of angles is related to the formation of TiO₂/Be (4%). Also, the reduced peak intensity after the addition of bentonite to titanium dioxide can be attributed to the coating of the titanium dioxide surface. The TiO₂/Be (4%) composite spectrum, in accordance with the standard PDF card of JCPDS 022-0502, includes a combination of silica, titanium, aluminum, and oxygen [22]. It is seen in Figure 1 that the structural spectrum of composites prepared with various zinc content is very similar to the titanium dioxide spectrum. In the TiO₂/Be/ZnO (6.5%) composite, the anatase phase of titanium dioxide is still seen as the dominant phase in the composition. The characteristic peaks of zinc oxide are located at 30°, 40°, 47°, 56°. But in the synthesized samples, because the composite has formed and the added material has penetrated the titanium dioxide structure, no additional peak that can be attributed to zinc oxide is seen. Also, given

that the amount of zinc used in the synthesis of composite samples is less than sufficient for the formation of zinc oxide phases, the zinc oxide phases have not appeared [23-24]. As the zinc oxide content increases in the samples prepared from 3.28% to 6.5%, the intensity of the characteristic peaks of the anatase phase related to titanium dioxide is increased. According to Figure 1, as the zinc oxide content exceeds 6.5%, the intensity of the peaks is reduced, especially the peaks related to the anatase phase. And it seems that the crystallinity of the network sharply declines. This phenomenon is probably due to the addition of extra zinc oxide to the network and the destruction of a part of the system's crystal structure. According to the diagram, 6.5% zinc oxide is optimum, where the anatase phase has the highest contribution to the crystalline phase. Besides, the crystallinity of the structure in this composition is greater than the other samples. The average size of the crystallites can be calculated based on the data obtained from the X-ray diffraction spectrum through the Debye-Scherrer equation $D = \frac{k\lambda}{\beta \cos \theta}$. In this equation, D is the average size of the crystallite (nm), K is the coefficient of the crystal shape (varying in the range of 0.62 to 2.08, and 0.9 on average), λ is the X-ray wavelength (copper lamp = 0.15406 nm), β is the peak width at the half of maximum height (FWHM) (radian), and θ is the diffraction angle (radian). The average size of the crystallites for the samples of titanium dioxide, bentonite, and composite TiO₂/Be/ZnO (6.5%) was equal to 49.94, 64.16, and 10.34 nm, respectively. XRF analysis is used to investigate the elemental analysis of the synthesized samples. Table 2 shows the content of constituting elements of composite TiO₂/Be/ZnO (6.5%) and the samples of titanium dioxide and bentonite. According to Table 2, in TiO₂/Be/ZnO (6.5%) composite, after titanium, the largest amount is assigned to zinc, silicon, and aluminum compared to other elements. These results, along with the results of XRD, show that the components of bentonite and zinc have entered the titanium dioxide structure, and the composite is well-formed.

Table 2. XRF elemental analysis of synthesized TiO₂, Bentonite and TiO₂/Be/ZnO (6.5%).

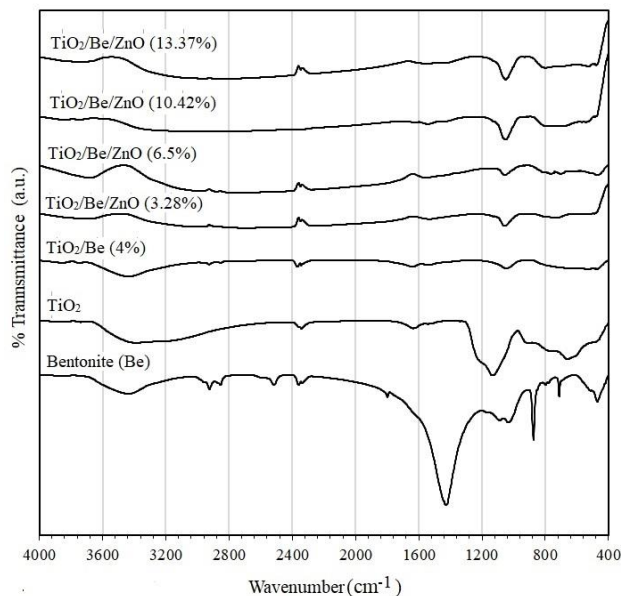
Elements	photocatalyst		
	TiO ₂	Be	ZnO/Be/TiO ₂
S	-	0.860	0.233
Mg	-	4.265	0.439
P	-	0.052	0.030
Ti	99.888	0.344	81.222
K	-	1.496	0.198
Ca	-	2.824	0.189
Fe	-	7.636	0.384
Al	-	13.655	1.427
Si	-	47.466	5.543
Zn	-	-	6.476
L.O.I.	0.112	21	3

3.1.2. Fourier transform spectrometry

Figure 2 shows the FT-IR spectra of TiO₂, bentonite, and the TiO₂/Be (4%) and TiO₂/Be/ZnO composites with different zinc contents. In the FT-IR spectrum of titanium dioxide, the peak observed in the 1066 cm⁻¹ region shows the stretching vibrations of the O-Ti-O band. The peak of 1480 cm⁻¹ is the bending vibration of Ti-O in the titanium dioxide network [27-25]. The broad peak in 1684 cm⁻¹ is attributed to the absorption of water molecules by the sample. In the raw bentonite spectrum, the peak observed in the 471 cm⁻¹ and 514 cm⁻¹ regions are related to the vibrations of Si-O-Si and Al-O-Si bonds, respectively [13]. The peaks observed in regions 712 cm⁻¹, 794 cm⁻¹, 847 cm⁻¹ are related to quartz vibrations in the sample. The stretching vibrations of the Si-O bond in the bentonite sample are seen in the 1028 cm⁻¹ region. The appearance of three peaks in 2364 cm⁻¹, 2514 cm⁻¹, and 2873 cm⁻¹ can be attributed to the presence of calcium [21]. A relatively high peak observed in the 3400 cm⁻¹ can be attributed to the stretching vibration of the OH group [26,21].

In the FT-IR spectrum of the TiO₂/Be composite, the peak of 490 cm⁻¹ shows the metal-oxygen bond. The peak in 1120 cm⁻¹ is related to the tensile vibrations of the O-Ti-O bond in the synthesized composite. As seen in the FT-IR spectrum of titanium dioxide, the peak of O-Ti-O is located at the 1066 cm⁻¹ region. But for the synthesized TiO₂/Be sample, the peak shifts to 1120, and this indicates the specific chemical interactions between TiO₂ and bentonite [28-27]. In the FT-IR spectrum of the TiO₂/Be/ZnO

composite, the peak observed in 490 cm⁻¹ is related to the vibrations of the metal-oxygen bond. In a sample synthesized with 6.5% zinc nitrate, the metal-oxygen bond is formed (M-O-M (M: Ti, Zn, Al, or Si)). As different values increase from the Zn source to the composite, the weak peaks appear at 530 cm⁻¹ up to the 610 cm⁻¹ regions, which characterizes the presence of zinc in the composition [28,22]. Due to the low content of zinc compared to titanium dioxide in the composite, the intensity of these peaks is very small.

**Fig. 2.** FT-IR spectra of synthesized samples.

3.1.3. FE-SEM analysis

Field emission scanning electron microscopy was used to determine the morphology of the synthesized particles. Figure 3 shows the FE-SEM image of titanium dioxide and the TiO₂/Be (4%) and TiO₂/Be/ZnO composites with different zinc content. According to Figure 3, the synthesized titanium dioxide particles are distributed uniformly and spherically. The surface of the spheres is very smooth and homogeneous. In the FE-SEM image of the synthesized TiO₂/Be (4%) composite, the uniform distribution of TiO₂ and bentonite particles can be detected, and the bentonite particles are located on the titanium dioxide surface. In this image, the TiO₂ particles spherically are reduced compared to the pure TiO₂ image. According to the results obtained by the researchers, the zinc oxide particles are spherical or flower-like alone [29], but with the composition of

these particles with the TiO_2/Be sample, its morphology is completely changed. In the SEM study, the distribution of the ZnO species on the TiO_2/Be sample can be seen where the surface of the sample is covered with ZnO particles, and there are no significant changes in sample morphology after the addition of ZnO. As seen from the SEM images, the ZnO particles are like clusters that are connected to the sample surface.

3.1.4. Thermogravimetric analysis

In order to determine the thermal stability of the composites, thermogravimetric analysis (TGA) was carried out for each of the samples. All the analyses were conducted in atmospheric air at 50–800°C at 10°C/min. The analysis shows the proportion of the physical and chemical changes of the composition proportional to the increase in temperature [32–33]. Figure 4 shows the TGA diagram of titanium dioxide and $\text{TiO}_2/\text{Be}/\text{ZnO}$ composites with various contents of zinc. For the synthesized TiO_2 sample, the amount of weight loss is attributed to the removal of ethanol and volatile matter. The data of this diagram show that about 90% of TiO_2 metal oxide remains stable at temperatures above 550 °C. Given the TGA diagrams for the $\text{TiO}_2/\text{Be}/\text{ZnO}$ composites with different zinc content, more weight loss occurs as the zinc content to the composites is increased, despite the constant thermal stability at temperatures above 600°C.

According to the results, with the increase in zinc content in the composite from 3.28%, 6.5%, 10.42%, 13.37%, the weight loss in the composites is 13%, 17%, 22%, and 33%, respectively. According to the diagram, three steps of weight loss are seen in these samples. The first step occurs with about 5% weight loss in the temperature range of 50–180°C. This step is attributed to the removal of surface water molecules. The relatively fast weight loss in the temperature range of 300–350°C is related to the decomposition of organic matter, loss of volatile matter, breakdown of $\text{Zn}(\text{OH})_2$

bond, and loss of the OH_2 group. Also, the mass loss at temperatures above 400°C is attributed to the loss of carbon in the sample. Besides, due to the loss of volatile matter and the conversion of titanium hydroxide to titanium dioxide, a similar and almost stable thermal stability trend at temperatures above 550°C can be seen in various synthesized samples. The results are consistent with the results of other articles [37–34].

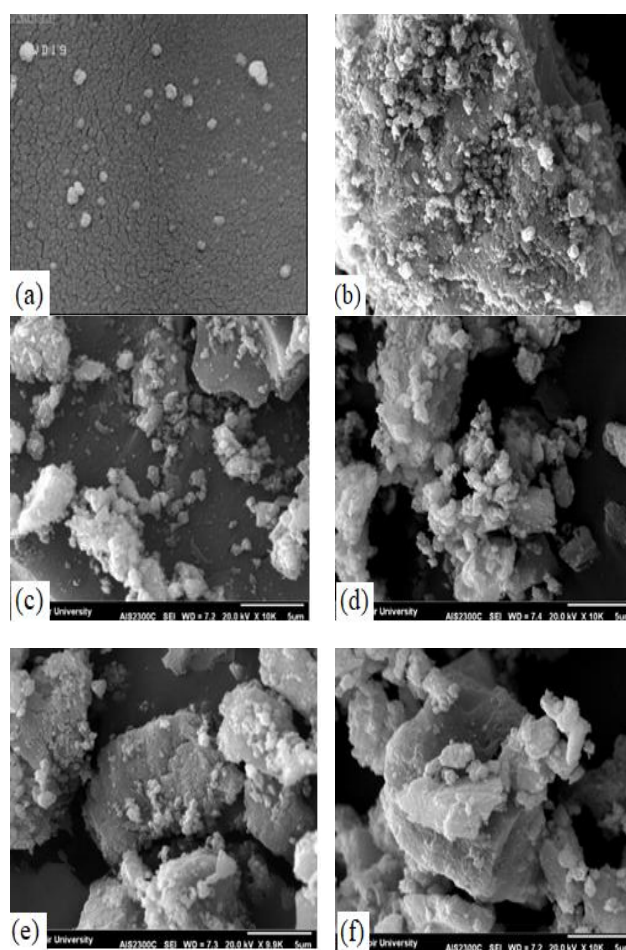


Fig. 3. FE-SEM images of synthesized samples: (a) TiO_2 , (b) TiO_2/Be (4%), (c) $\text{TiO}_2/\text{Be}/\text{ZnO}$ (3.28%), (d) $\text{TiO}_2/\text{Be}/\text{ZnO}$ (6.5%), (e) $\text{TiO}_2/\text{Be}/\text{ZnO}$ (10.42%), and (f) $\text{TiO}_2/\text{Be}/\text{ZnO}$ (13.37%).

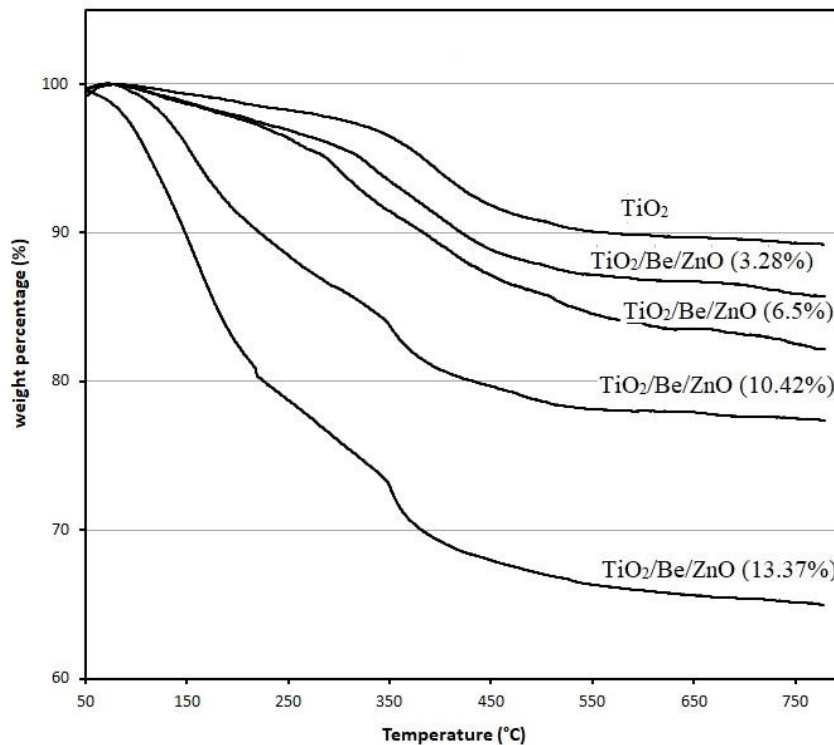


Fig. 4. TGA curves of synthesized samples.

3.2. Photocatalysis experiments

3.2.1. Choosing the suitable photocatalyst

The type of photocatalyst is the most effective parameter in the photocatalytic degradation of dye. In fact, by exposing a photocatalyst such as TiO_2 to light, the photocatalyst absorbs the photon energy, which makes the electrons move from the valence band to the conduction band. Therefore, a positive hole is made in the valence band. And as a result of the reaction with the hydroxyl groups in the environment, free radical hydroxyl is produced, which is a strong oxidizing agent and is considered a destructive agent of dye organic pollutants. Moreover, these electrons can also react with the O_2 in the water-soluble titanium and convert to the radical superoxide anion (O_2^-). In Table 3, the results of the photocatalytic experiments of the titanium dioxide samples, TiO_2/Be (4%), and various $\text{TiO}_2/\text{Be}/\text{ZnO}$ composites are shown. According to the results of Table 3, the photocatalytic removal of methyl orange is increased from 57.82% to 78.81% with the addition of 4 wt% bentonite to pure titanium dioxide. An explanation is as follows. In the photocatalytic degradation of pollutants, a large number of

electron-hole pairs are recombined, which reduces the process efficiency. It seems that the doping of titanium dioxide with bentonite that mainly consists of aluminum and silicon oxides improves the intermediate charge transfer reaction and delays the return of the electrons of the conduction band to the TiO_2 valence band and prevents the electron-hole recombination; as a result, the photocatalyst performance is significantly increased.

Table 3. The performance of different photocatalyst for degradation of methyl orange at same conditions.

photocatalyst	Amount of Be (%)	Amount of ZnO (%)	Degradation percentage (%)
TiO_2	-	-	57.82
TiO_2/Be (4%)	4	-	78.81
$\text{TiO}_2/\text{Be}/\text{ZnO}$ (3.28%)	4	3.28	82
$\text{TiO}_2/\text{Be}/\text{ZnO}$ (6.5%)	4	6.5	98
$\text{TiO}_2/\text{Be}/\text{ZnO}$ (10.42%)	4	10.42	80
$\text{TiO}_2/\text{Be}/\text{ZnO}$ (13.37%)	4	13.37	78

Conditions: dosage of photocatalyst: 4 g/L; dye concentration: 10 ppm; irradiation time: 60 min.

According to the results of Table 3, the addition of different values of zinc nitrate to TiO_2/Be (4%) and the production of various $\text{TiO}_2/\text{Be}/\text{ZnO}$ composites increase the photocatalytic removal efficiency of methyl orange. In fact, with the addition of zinc oxide to the titanium dioxide semiconductor, which has a larger band gap than titanium dioxide, the electrons that are separated in the first step and created a hole are trapped by the second (bentonite) and third (zinc oxide) catalyst surfaces, providing more time for oxidation-reduction and pollutant degradation reactions. As a result, the photocatalytic removal of methyl orange dye in the presence of a synthesized composite with 6.5% zinc oxide content shows better performance (98%) compared to other composites synthesized with values of 3.28%, 10.42%, 13.37%. According to the results obtained from the XRD spectrum, with an increase of zinc oxide from 3.28% to 6.5% in the synthesized samples of $\text{TiO}_2/\text{Be}/\text{ZnO}$, the intensity of the characteristic peaks of the anatase phase related to titanium dioxide is increased; then, with an increase in the zinc oxide content up to 13.37%, the intensity of the characteristic peaks of anatase phase related to titanium dioxide is reduced. According to the results reported by other researchers, among different phases of titanium dioxide, the anatase phase has the highest photocatalytic property, which is consistent with our photocatalytic results [38]. Moreover, in examining the FT-IR spectrum of samples, only in the sample synthesized with 6.5% zinc, the weak characteristic peaks of zinc oxide are visible at the 530 to 610 regions. Given that the sample synthesized with 6.5% zinc oxide has the highest photocatalytic removal efficiency than other photocatalysts, the simultaneous effect of parameters affecting photocatalyst degradation of methyl orange is evaluated in the presence of $\text{TiO}_2/\text{Be}/\text{ZnO}$ (6.5%) using the RSM method.

3.2.2. Investigating the results of experiment design by RSM

3.2.2.1. Analysis of variance

Analysis of variance is the most widely used technique for statistical results. Using ANOVA, the

models presented for the prediction of responses were investigated, and the regression coefficients were estimated for linear terms, second-order terms, and interaction terms. Design-Expert software examines the suitability and validity of the model by ANOVA using the three parameters of R-square (R^2), Fisher test (F-test), and probability (P-value). Table 4 shows the ANOVA results for methyl orange dye degradation in the presence of $\text{TiO}_2/\text{Be}/\text{ZnO}$ (6.5%). The R-square determines the quality of model fitting. The adjusted R-squared (R_{adj}^2) is the modified state of R-square, and it is reduced if unnecessary factors are added to the model. In fact, R^2 is obtained from the sum of the squares of the difference between the experimental and the predicted values. And the closer the value to one, the better match between the experimental data and predicted model data occurred. The values of R^2 and R_{adj}^2 obtained from these experiments are 0.9072 and 0.8718, respectively, which shows that the model properly predicts the experimental data. Statistically, a model that has the highest adjusted R-squared is suitable. This condition is necessary but not sufficient for the detection of precision. The significance of the models is statistically analyzed with the F and P values. The larger F value shows the higher validity of the model. Furthermore, along with a larger F value, the smaller P value (<0.0001) related to the model indicates that the model properly predicts the experimental data. The P-value determines the effective terms. If P-value < 0.05 for a model term, that term is an effective parameter on response. According to the results, the irradiation time (B), dye concentration (C), amount of catalyst (A), and pH (D) are among the effective parameters on the response equation that represents the dye degradation. According to the results, the interaction between the parameters is not important and has no serious impact on dye degradation.

Table 4. ANOVA table for response surface squares model for degradation percentage of methyl orange.

Source	Sum of squares	Degree of freedom	Mean	F value	p-Value prob > F
Model	10675.07	8	1334.38	25.65	<0.0001
A	1574.48	1	157.48	30.26	<0.0001
B	5816.02	1	5816.02	111.7	<0.0001
C	2460.58	1	2460.58	47.29	<0.0001
D	673.84	1	673.84	12.95	0.0017
AB	28.70	1	28.70	0.55	0.4659
AC	0.072	1	0.072	1.375E-003	0.9708
BC	121.28	1	121.28	2.33	0.1417
BD	0.11	1	0.11	2.06E-003	0.9642
Lack of fit	1092.59	16	68.29	-	-
Pure error	0.000	5	-	-	-
Residual	1092.59	21	52.03	-	-
Total	11767.66	29	-	-	-

$R^2 = 0.9072$, R^2 (adjusted) = 0.8718, R^2 (predicted) = 0.8034.

Using ANOVA, the polynomial model No. 1 is obtained to predict the photocatalytic degradation percentage of methyl orange. In this equation, R is the degradation percentage of methyl orange. Given the coefficients of the equation parameters, the parameters (B), (C), (A), and D have the greatest effect on the response equation. According to the negative sign of the parameters B and D, the dye degradation is reduced with an increase in the value of parameters B and D. also based on the positive sign of the parameters A and C, the dye degradation is increased with an increase in parameters A and C.

$$R = 51.72 + 8.10A - 15.57B + 10.13C - 5.30D - 1.34AB + 0.067AC - 2.57BC + 0.082BD \quad (1)$$

In Figure 5, the data predicted by the model are shown based on the experimental data. According to Figure 5, the experimental and predicted values are close enough to the bisector line of the axes; this indicates that the predicted values are slightly distracted from the experimental data, and a proper regression of experimental data is performed. And the model is quite reliable. Figure 6 indicates the random dispersion of points in the residuals range. In this diagram, if the data are dispersed between two fixed points with no particular trend, the model is suitable. In these diagrams, the data are normally distributed with a power transfer function in the studentized range. As a result, a proper randomized dispersion is seen in the studentized range. Figure 7 shows the diagram of normal probability changes based on studentized residuals. The vector will be

normal in the state where the points are linearly placed on the normalization line, but if the points are s-shaped in the line range, the diagram shows no normal distribution [39]. According to Figure 7, the normal diagram shows that residual values are normal and have an independent distribution, which shows that the model has a proper precision, the error values have a normal distribution, and the resulting data have no noise.

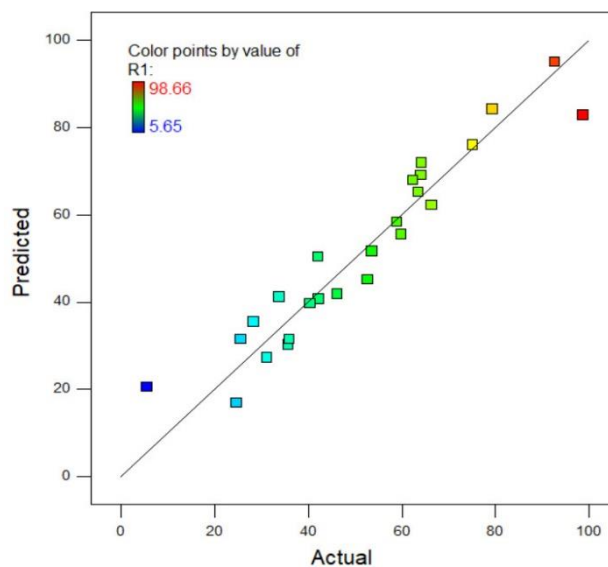


Fig. 5. A rough comparison between the predicted values for methyl orange degradation against the experimental data (Actual data) for $\text{TiO}_2/\text{Be}/\text{ZnO}$ (6.5%) as photocatalyst.

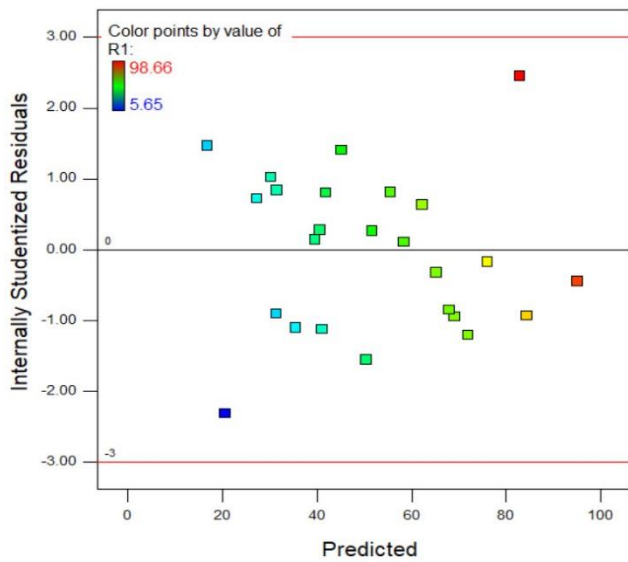


Fig. 6. Residual versus predicted plot for methyl orange degradation over $\text{TiO}_2/\text{Be}/\text{ZnO}$ (6.5%) as photocatalyst.

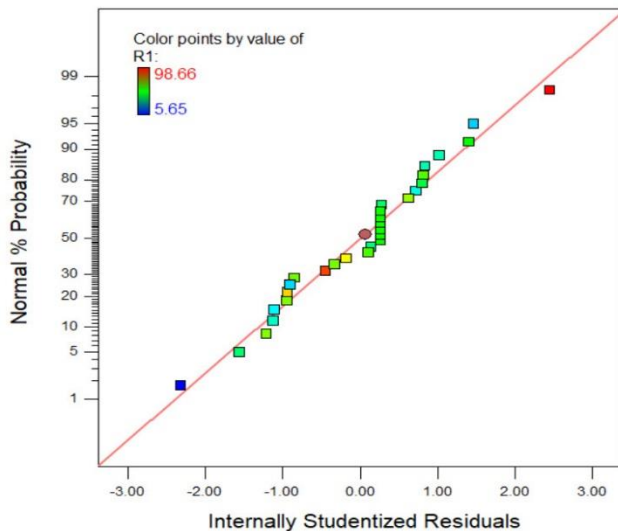


Fig. 7. The calculated dependence of the normal probability on internally studentized residuals for methyl orange degradation.

3.2.2.2. Investigating the effect of parameters on photocatalytic degradation

Figure 8 shows a 3D diagram of the simultaneous effect of dye concentration and catalyst concentration on methyl orange degradation. According to Figure 8, the dye degradation increases with an increase in photocatalyst concentration. In fact, there are not enough active and unsaturated positions at low concentrations of the photocatalyst, but with an increase in photocatalyst concentration, the amount of available active positions is increased for dye molecules. However,

constantly increasing the photocatalyst concentration is not always in favor of the amount of degradation. By increasing the photocatalyst concentration greater than the optimal value, the agglomeration of photocatalyst is occurred and then the available active site of catalyst are reduced that caused the reduction in degradation efficiency. Also by increasing the photocatalyst concentration greater than the optimal value, the turbidity of solution was increased that caused the reduction in light penetration. As a result, reducing the penetration of light reduces the efficiency of the degradation process. Also, in accordance with this figure, the highest degradation is seen at high concentrations of the dye in the examined range. At high dye concentrations, with a decrease in the available absorption points, the catalytic activity is reduced; however, in this work, the range of dye concentrations was low, and the degradation of dye increased with increasing dye concentration. Figure 9 shows the simultaneous effect of time of radiation and pH on the methyl orange dye degradation. According to the figure, increasing the time of photon radiation has a negative effect on photocatalytic dye degradation in our time range. The light radiation causes the excitation of the electrons and the production of free radicals. The free radicals lead to the destruction of methyl orange with the oxidation of the pollutants. According to Figure 8, it is clearly seen that the amount of degradation decreases as the time of radiation increases. It seems that the recombination of free radicals increases, and as a result, the amount of dye degradation from the solution decreases. The effect of pH on photocatalytic degradation efficiency of methyl orange is shown in Figure 9. The photocatalytic degradation efficiency is affected by TiO_2 surface charge, dye molecule charge, dye absorption on TiO_2 surface, and radical hydroxyl concentration; all of these properties are dependent on the pH of the solution. Given that methyl orange dye is anionic, the H^+ concentration is high in the acidic pH, and H^+ ions of the catalyst surface have a positive charge. As a result, the electrostatic gravity increases between the methyl orange dye and the catalyst surface, and a greater amount of methyl orange is absorbed with the catalyst surface and degraded in the electron-hole process. In the alkaline environment, due to the

presence of the hydroxyl group, the catalyst surface is negated, and the repulsion created between the catalyst surface and anionic methyl orange adsorption is reduced. Therefore, the photocatalytic degradation of methyl orange decreases. The results are consistent with the results of other researchers [40-41]. The achievement of optimal conditions for variables affecting the process is one of the experimental design objectives. The optimization results showed that the maximum degradation efficiency of methyl orange in the presence of the $\text{TiO}_2/\text{Be}/\text{ZnO}$ (6.5%) photocatalyst at pH=5, 0.1g of photocatalyst, dye concentration of 20 ppm, and duration of 30 min was equal to 95%. A test was conducted in optimal conditions to ensure the optimum results of the model. The result of the methyl orange degradation test at optimal conditions was 94.1%, which was in good agreement with the degradation of methyl orange predicted by the model in optimal conditions. The photocatalyst reusability is a very important parameter in the applicability evaluation of the

photocatalyst. In fact, the reuse of a photocatalyst is very important with respect to the reduced losses of the process. To examine the possibility of reuse of synthesized catalyst, 4g/L of catalyst was added to 25 mL of 10 ppm solution of methyl orange and exposed to the visible light radiation for 60 min. After the end of the reaction, the catalyst was separated from the reaction mixture using the centrifuge, rinsed twice with distilled water, and dried for 24 hours. After complete drying, the catalyst was reused in the dye degradation reaction in the same conditions, and the above steps were repeated. This process was repeated five times, and the final dye concentration at each step was measured by UV-Vis spectrophotometry. The results are presented in Table 5. According to the results, the photocatalytic activity of $\text{TiO}_2/\text{Be}/\text{ZnO}$ (6.5%) in certain conditions, for reuse in five consecutive steps, shows a slight decrease (about 22% and similar to previous studies by the other researchers) in the degradation of methyl orange. Hence, the synthesized composite will be reusable [27,42].

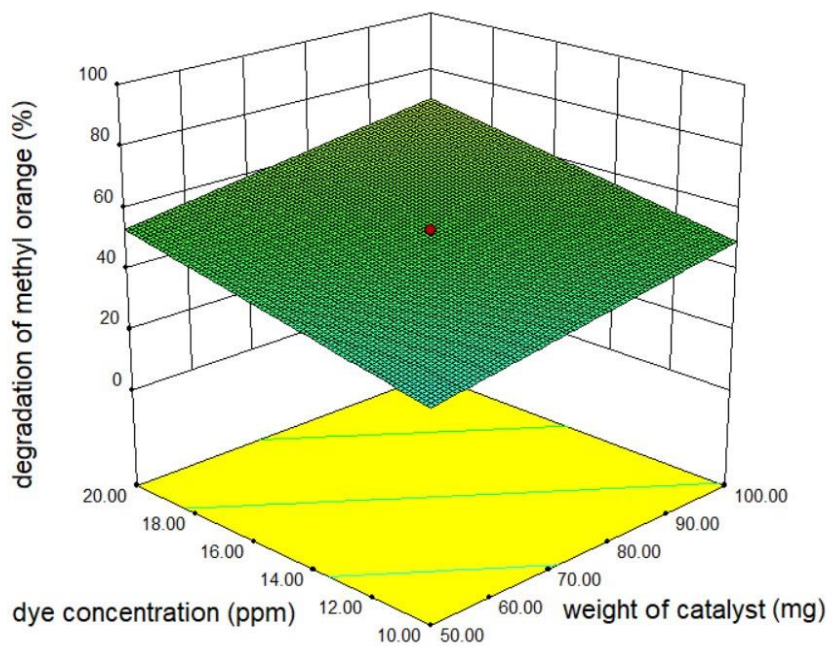


Fig. 8. 3D diagram of simultaneous effect of dye concentration and weight of catalyst on degradation of methyl orange.

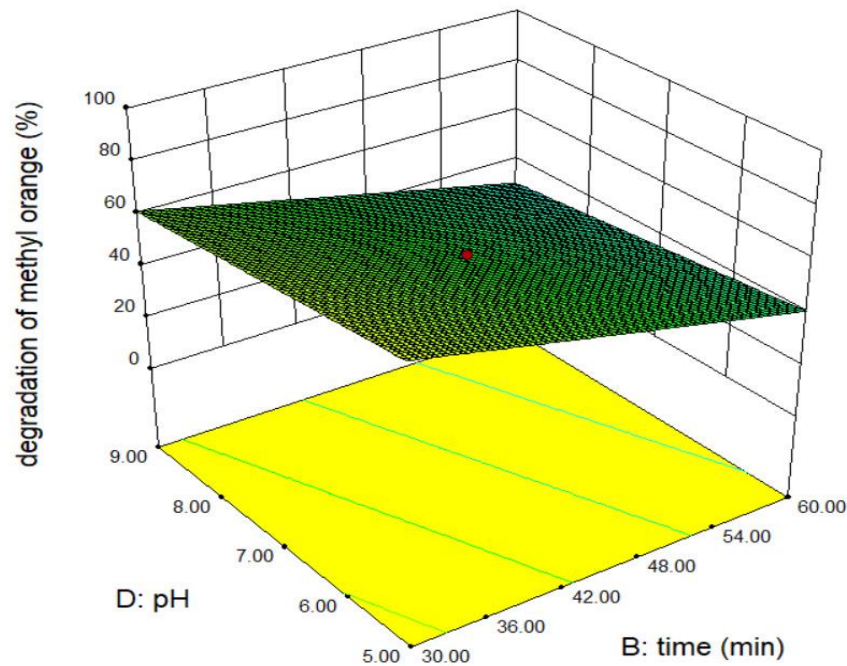


Fig. 9. 3D diagram of simultaneous effect of time of radiation and pH of solution on degradation of methyl orange.

Table 5. Reusability of the $\text{TiO}_2/\text{Be}/\text{ZnO}$ in photodegradation of methyl orange.

Run	Degradation percentage
1	96
2	82.5
3	76.43
4	75.4
5	74.26

Conditions: dosage of photocatalyst: 4 g/L; dye concentration: 10 ppm; pH: 6; irradiation time: 60 min.

4. Conclusions

In this research, $\text{TiO}_2/\text{Be}/\text{ZnO}$ photocatalysts were synthesized with different contents of ZnO and identified by XRD, FT-IR, FE-SEM, and TGA. The results of XRD showed that in the sample synthesized with 6.5% ZnO, the anatase phase had the highest contribution to the crystalline phase. Also, the crystallinity of the structure in this composition was higher than the other samples. To investigate the photocatalytic activity of the synthesized samples, the photocatalytic degradation of the methyl orange dye pollutant was studied. For the experimental design, the central composite design under the response surface method was used by Design Expert software. The effect of four parameters, including dye concentration, duration of light exposure, concentration of catalyst, and pH, on the degradation of methyl orange dye was

investigated. The results showed that the $\text{TiO}_2/\text{Be}/\text{ZnO}$ composite with 6.5% zinc oxide had the highest degradation efficiency of methyl orange. In the analysis of parameters affecting the photocatalytic degradation process, it was found that the catalyst concentration and radiation time had the highest effect on the degradation of the dye. Using the obtained model, the optimal conditions for the photocatalytic tests of $\text{TiO}_2/\text{Be}/\text{ZnO}$ (6.5%) composite were the dye concentration of 20 ppm, catalyst concentration of 100 mg, pH=5, and duration of 30 min; the methyl orange degradation of 95% was consistent with the experimental data. The results obtained from the analysis of the reusability of the composites as photocatalysts showed that using the synthesized composite for five consecutive times reduced its photocatalytic activity by almost 22%, which indicated that the synthesized composite would be reusable.

References

- [1] Bhattacharyya, R., Ray, S. K. (2015). Removal of congo red and methyl violet from water using nano clay filled composite hydrogels of poly acrylic acid and polyethylene glycol. *Chemical engineering journal*, 260, 269-283.
- [2] Jauris, I. M., Fagan, S. B., Adebayo, M. A., Machado, F. M. (2016). Adsorption of acridine orange and methylene blue synthetic dyes and

- anthracene on single wall carbon nanotubes: a first principle approach. *Computational and theoretical chemistry*, 1076, 42-50.
- [3] Rahimi, M., Mahmoudi, J. (2017). Studies on optimization of efficient parameters for removal of lead from aqueous solutions by natural zeolite as a low-cost adsorbent using response surface methodology. *Advances in environmental technology*, 3(2), 99-108.
- [4] Yilmaz, A. E., Boncukcuoğlu, R., Kocakerim, M., Karakaş, İ. H. (2011). Waste utilization: The removal of textile dye (Bomplex Red CR-L) from aqueous solution on sludge waste from electrocoagulation as adsorbent. *Desalination*, 277(1-3), 156-163.
- [5] Royer, B., Cardoso, N. F., Lima, E. C., Vaghetti, J. C., Simon, N. M., Calvete, T., Veses, R. C. (2009). Applications of Brazilian pine-fruit shell in natural and carbonized forms as adsorbents to removal of methylene blue from aqueous solutions—Kinetic and equilibrium study. *Journal of hazardous materials*, 164(2-3), 1213-1222.
- [6] Carneiro, P. A., Umbuzeiro, G. A., Oliveira, D. P., Zanoni, M. V. B. (2010). Assessment of water contamination caused by a mutagenic textile effluent/dyehouse effluent bearing disperse dyes. *Journal of hazardous materials*, 174(1-3), 694-699.
- [7] Rahimi, M., Mahmoudi, J. (2020). Heavy metals removal from aqueous solution by modified natural zeolites using central composite design. *Periodica polytechnica chemical engineering*, 64(1), 106-115.
- [8] Ban, J. J., Xu, G. C., Zhang, L., Lin, H., Sun, Z. P., Lv, Y., Jia, D. Z. (2017). Mesoporous ZnO microcube derived from a metal-organic framework as photocatalyst for the degradation of organic dyes. *Journal of solid state chemistry*, 256, 151-157.
- [9] Zhu, X. D., Zheng, Y. L., Feng, Y. J., Sun, K. N. (2018). Delicate Ag/V₂O₅/TiO₂ ternary nanostructures as a high-performance photocatalyst. *Journal of solid state chemistry*, 258, 691-694.
- [10] Hosseini, S. N., Borghei, S. M., Vossoughi, M., Taghavinia, N. (2007). Immobilization of TiO₂ on perlite granules for photocatalytic degradation of phenol. *Applied catalysis B: environmental*, 74(1-2), 53-62.
- [11] Asvadi, F., Fallah, N., Elyasi, S., Mohseni, F. (2017). Investigation of affecting operational parameters in photocatalytic degradation of reactive red 198 with TiO₂: optimization through response surface methodology. *Advances in environmental technology*, 2(4), 169-177.
- [12] Mahmoodi, N. M., Arami, M., Limaee, N. Y., Gharanjig, K., Ardejani, F. D. (2006). Decolorization and mineralization of textile dyes at solution bulk by heterogeneous nanophotocatalysis using immobilized nanoparticles of titanium dioxide. *Colloids and surfaces A: physicochemical and engineering aspects*, 290(1-3), 125-131.
- [13] Zyoud, A., Jondi, W., AlDaqqah, N., Asaad, S., Qamhieh, N., Hajamohideen, A., Hilal, H. S. (2017). Self-sensitization of tetracycline degradation with simulated solar light catalyzed by ZnO@ montmorillonite. *Solid state sciences*, 74, 131-143.
- [14] Kitano, M., Matsuoka, M., Ueshima, M., Anpo, M. (2007). Recent developments in titanium oxide-based photocatalysts. *Applied catalysis A: general*, 325(1), 1-14.
- [15] Tian, J., Wang, J., Dai, J., Wang, X., Yin, Y. (2009). N-doped TiO₂/ZnO composite powder and its photocatalytic performance for degradation of methyl orange. *Surface and coatings technology*, 204(5), 723-730.
- [16] Huang, M., Xu, C., Wu, Z., Huang, Y., Lin, J., Wu, J. (2008). Photocatalytic discolorization of methyl orange solution by Pt modified TiO₂ loaded on natural zeolite. *Dyes and pigments*, 77(2), 327-33..
- [17] Li, F., Jiang, Y., Yu, L., Yang, Z., Hou, T., Sun, S. (2005). Surface effect of natural zeolite (clinoptilolite) on the photocatalytic activity of TiO₂. *Applied surface science*, 252(5), 1410-1416.
- [18] Habib, M. A., Shahadat, M. T., Bahadur, N. M., Ismail, I. M., Mahmood, A. J. (2013). Synthesis and characterization of ZnO-TiO₂ nanocomposites and their application as photocatalysts. *International nano letters*, 3(1), 1-8.
- [19] Krysa, J., Keppert, M., Jirkovsky, J., Stengl, V., Subrt, J. (2004). The effect of thermal treatment on the properties of TiO₂

- photocatalyst. *Materials chemistry and physics*, 86(2-3), 333-339.
- [20] Moradi, S., Aberoomand Azar, P., Raeis Farshid, S., Abedini Khorrami, S., Givianrad, M. H. (2012). Effect of Additives on Characterization and Photocatalytic Activity of TiO₂/ZnO Nanocomposite Prepared via Sol-Gel Process. *International journal of chemical engineering*, 215373.
- [21] Hayati-Ashtiani, M. (2012). Use of FTIR spectroscopy in the characterization of natural and treated nanostructured bentonites (montmorillonites). *Particulate science and technology*, 30(6), 553-564.
- [22] Zhang, G. K., Ding, X. M., He, F. S., Yu, X. Y., Zhou, J., Hu, Y. J., Xie, J. W. (2008). Low-temperature synthesis and photocatalytic activity of TiO₂ pillared montmorillonite. *Langmuir*, 24(3), 1026-1030.
- [23] Samadi, S., Motallebi, R., Nasiri Nasrabadi, M. (2016). Synthesis, characterization and application of Lanthanide metal-ion-doped TiO₂/bentonite nanocomposite for removal of Lead (II) and Cadmium (II) from aquatic media. *Journal of water and environmental nanotechnology*, 1(1), 35-44.
- [24] Sakthivel, S., Neppolian, B., Shankar, M. V., Arabindoo, B., Palanichamy, M., Murugesan, V. (2003). Solar photocatalytic degradation of azo dye: comparison of photocatalytic efficiency of ZnO and TiO₂. *Solar energy materials and solar cells*, 77(1), 65-82.
- [25] Zhang, X., Yao, B., Zhao, L., Liang, C., Zhang, L., Mao, Y. (2001). Electrochemical fabrication of single-crystalline anatase TiO₂ nanowire arrays. *Journal of the electrochemical society*, 148(7), G398.
- [26] Rossetto, E., Petkowicz, D. I., dos Santos, J. H., Pergher, S. B., Penha, F. G. (2010). Bentonites impregnated with TiO₂ for photodegradation of methylene blue. *Applied clay science*, 48(4), 602-606.
- [27] Yener, H. B., Yılmaz, M., Deliismail, O., Ozkan, S. F., Helvacı, S. S. (2017). Clinoptilolite supported rutile TiO₂ composites: Synthesis, characterization, and photocatalytic activity on the degradation of terephthalic acid. *Separation and purification technology*, 173, 17-26.
- [28] Wang, X. T., Zhong, S. H., Xiao, X. F. (2005). Photo-catalysis of ethane and carbon dioxide to produce hydrocarbon oxygenates over ZnO-TiO₂/SiO₂ catalyst. *Journal of molecular catalysis A: chemical*, 229(1-2), 87-93.
- [29] Pal, S., Mondal, S., Maity, J., Mukherjee, R. (2018). Synthesis and characterization of ZnO nanoparticles using Moringa oleifera leaf extract: investigation of photocatalytic and antibacterial activity. *International journal of nanoscience and nanotechnology*, 14(2), 111-119.
- [30] Regulska, E., Brus, D. M., Rodziewicz, P., Sawicka, S., Karpinska, J. (2016). Photocatalytic degradation of hazardous Food Yellow 13 in TiO₂ and ZnO aqueous and river water suspensions. *Catalysis today*, 266, 72-81.
- [31] Bentouami, A., Ouali, M. S., De Menorval, L. C. (2010). Photocatalytic decolourization of indigo carmine on 1, 10-phenanthroline intercalated bentonite under UV-B and solar irradiation. *Journal of photochemistry and photobiology A: chemistry*, 212(2-3), 101-106.
- [32] Bunnak, N., Laoratanakul, P., Bhalla, A. S., Manuspiya, H. (2014). Surface-modified porous clay heterostructure synthesized by introduction of cationic ions: effects on dielectric behavior. *Ferroelectrics*, 473(1), 187-197.
- [33] Murariu, M., Doumbia, A., Bonnaud, L., Dechief, A. L., Paint, Y., Ferreira, M., Dubois, P. (2011). High-performance polylactide/ZnO nanocomposites designed for films and fibers with special end-use properties. *Biomacromolecules*, 12(5), 1762-177.
- [34] Liufu, S. C., Xiao, H. N., Li, Y. P. (2005). Thermal analysis and degradation mechanism of polyacrylate/ZnO nanocomposites. *Polymer degradation and stability*, 87(1), 103-110.
- [35] Nguyen, V. C., Nguyen, N. L. G., Pho, Q. H. (2015). Preparation of magnetic composite based on zinc oxide nanoparticles and chitosan as a photocatalyst for removal of reactive blue 198. *Advances in natural sciences: nanoscience and nanotechnology*, 6(3), 035001.
- [36] Zhu, H., Jiang, R., Fu, Y., Guan, Y., Yao, J., Xiao, L., Zeng, G. (2012). Effective photocatalytic decolorization of methyl orange utilizing TiO₂/ZnO/chitosan nanocomposite

- films under simulated solar irradiation. *Desalination*, 286, 41-48.
- [37] Wang, Q., Chen, K., Zhang, Y. (2016). Preparation of La-TiO₂/Bentonite and Its Photodegradation Properties to Cyanide. *Journal of nanoscience and nanotechnology*, 16(4), 4233-4238.
- [38] Wang, Q., Chen, K., Zhang, Y. (2016). Preparation of La-TiO₂/Bentonite and Its Photodegradation Properties to Cyanide. *Journal of nanoscience and nanotechnology*, 16(4), 4233-4238.
- [39] Chang, C. J., Yang, T. L., Weng, Y. C. (2014). Synthesis and characterization of Cr-doped ZnO nanorod-array photocatalysts with improved activity. *Journal of solid state chemistry*, 214, 101-107.
- [40] Muruganandham, M., Swaminathan, M. (2006). Photocatalytic decolourisation and degradation of Reactive Orange 4 by TiO₂-UV process. *Dyes and pigments*, 68(2-3), 133-142.
- [41] Padikkaparambil, S., Narayanan, B., Yaakob, Z., Viswanathan, S., Tasirin, S. M. (2013). Au/TiO₂ reusable photocatalysts for dye degradation. *International journal of photoenergy*, 752605.
- [42] Teixeira, S., Martins, P. M., Lanceros-Mendez, S., Kühn, K., Cuniberti, G. (2016). Reusability of photocatalytic TiO₂ and ZnO nanoparticles immobilized in poly (vinylidene difluoride)-co-trifluoroethylene. *Applied surface science*, 384, 497-504.